Table 2 Variables associated with the presence of advanced fibrosis (F3–4) by univariate and multivariate analysis

	F0–2 ($n = 83$)	F3–4 ($n = 32$)	*P*-value (Univariate)	Odds ratio (95% CI) (Multivariate)
Age (years)	56.6 ± 10.9	61.3 ± 10.4	0.03	
Sex (female/male)	51/32	17/15	0.41	
AST (IU/L)	52.3 ± 43.3	64.4 ± 48.3	0.19	
ALT (IU/L)	62.9 ± 60.6	63.9 ± 44.2	0.93	
Platelets ($\times 10^9$/L)	179 ± 47	117 ± 42	<0.001	0.78 (0.68–0.89)
LF index	2.81 ± 0.69	3.86 ± 0.81	<0.001	5.30 (2.16–13.0)

ALT, alanine aminotransferase; AST, aspartate aminotransferase; CI, confidence interval; LF, liver fibrosis.

Multivariate analysis showed that LF index was independently associated with the presence of minimal fibrosis (OR = 0.25, 95% CI = 0.11–0.55).

Diagnostic accuracy of RTE and serum fibrosis markers

Receiver-operator curves of LF index, platelets, FIB-4 index and APRI for predicting advanced fibrosis (F3–4), and minimal fibrosis (F0–1) were plotted, as shown in Figure 4. AUROC of LF index for predicting advanced fibrosis (0.84) was superior to platelets (0.82), FIB-4 index (0.80) and APRI (0.76). Similarly, for predicting minimal fibrosis, AUROC of LF index (0.81) was superior to platelets (0.73), FIB-4 index (0.79) and APRI (0.78). The corresponding sensitivities, specificities, PPV and NPV are detailed in Table 4.

DISCUSSION

IMPROVEMENTS IN VARIOUS methods for prediction of liver fibrosis have recently emerged as alternatives to liver biopsy. RTE is a non-invasive method for the measurement of tissue elasticity using ultrasonography. The utility of RTE for evaluating liver fibrosis is reported in a few studies.[18–22] However, for utilizing LF index, one of the equations used to calculate tissue elasticity by RTE is still unclear. The aim of this study was to investigate the significance of LF index for the prediction of liver fibrosis in CHC patients.

In this prospective study, we found that LF index is a useful predictive factor for diagnosis of the fibrosis stage in CHC patients. Increase in LF index significantly correlated with progression of the fibrosis stage and LF index was able to predict the presence of advanced fibrosis and minimal fibrosis. Previous studies reported the utility of LF index for prediction of the liver fibrosis stage.[21,22] In this study, LF index differed significantly between patients with F0–1 and F2; thus, LF index was especially useful for prediction of minimal fibrosis. This may be due to a sufficient number of patients with F0–1 and F2 included in the present study. This is an advantage of LF index because other quantitative methods by RTE could not discriminate patients with F0–1 and F2.[19,20] On the other hand, there is a possibility that a similar result may be obtained for differentiation of F3 and F4 if a large number of patients with advanced fibrosis was included.

Previous studies did not compare the diagnostic accuracy of LF index and serum fibrosis markers. We revealed that LF index performed better than serum fibrosis

Table 3 Variables associated with the presence of minimal fibrosis (F0–1) by univariate and multivariate analysis

	F0–1 ($n = 51$)	F2–4 ($n = 64$)	*P*-value (Univariate)	Odds ratio (95% CI) (Multivariate)
Age (years)	54.0 ± 11.9	61.0 ± 9.0	<0.001	
Sex (female/male)	31/20	37/27	0.74	
AST (IU/L)	44.5 ± 42.6	64.6 ± 44.9	0.02	
ALT (IU/L)	53.0 ± 56.3	71.3 ± 55.5	0.08	
Platelets ($\times 10^9$/L)	186 ± 47	142 ± 50	<0.001	
LF index	2.60 ± 0.59	3.51 ± 0.84	<0.001	0.25 (0.11–0.55)

ALT, alanine aminotransferase; AST, aspartate aminotransferase; CI, confidence interval; LF, liver fibrosis.

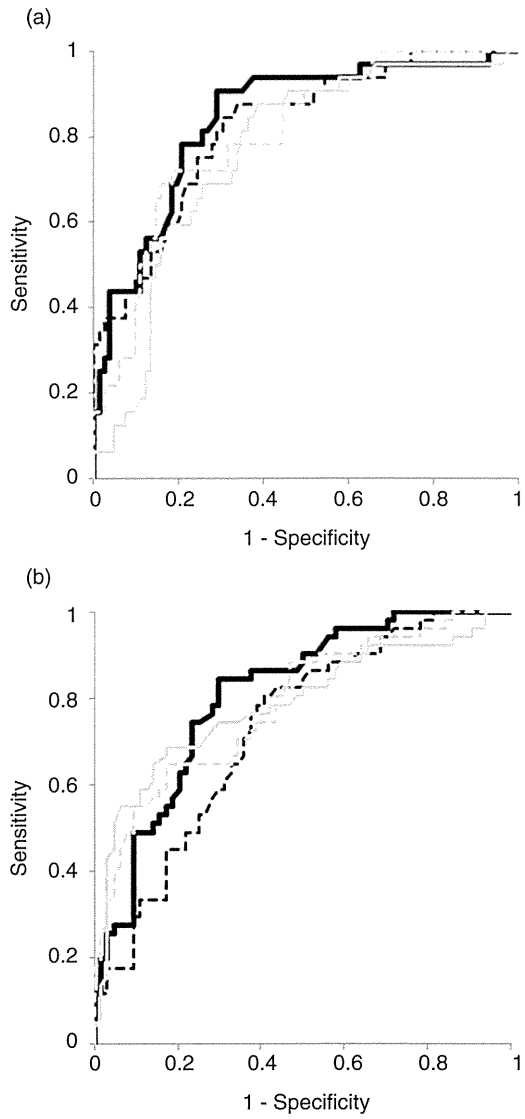

Figure 4 Receiver–operator curves (ROC) of liver fibrosis (LF) index and serum fibrosis markers. (a) ROC for diagnosis of significant fibrosis (F3–4). (b) ROC for diagnosis of minimal fibrosis (F0–1). —, LF index; ····, platelets; ——, aspartate aminotransferase-to-platelet ratio index; – –, FIB-4 index.

markers based on blood laboratory tests for predicting liver fibrosis.

Transient elastography has been most commonly used to measure liver stiffness and is established in clinical practice to evaluate liver fibrosis.[8,9] RTE exhibits some advantages compared with transient elastography. In this study, RTE imaging was successfully performed in all patients, and LF index was calculated. Although transient elastography has high diagnostic capabilities when it comes to liver fibrosis, measurements are sometimes impossible in patients with severe obesity and ascites.[24] Reproducibility of transient elastography was reportedly lower in patients with steatosis, inflammation, increased body mass index and lower degrees of liver fibrosis.[25–27] On the other hand, LF index is measured by ultrasound guidance that facilitates the identification of a suitable location for elastographic measurement, thereby resulting in a higher number of patients with valid results.

Unlike transient elastography, another advantage of LF index is that the results are not influenced by the presence of inflammation and steatosis. It was reported that LF index is not useful in patients with steatosis.[22] However, LF index was not significantly different between patients with and without steatosis in the present study even after stratification by fibrosis stage. Thus, LF index was useful for prediction of fibrosis in CHC patients regardless of steatosis. Because LF index of each activity grade and steatosis grade did not differ from each other, estimation of liver fibrosis by LF index demonstrated higher reproducibility than transient elastography.

In previously reports, diagnostic accuracy of liver fibrosis using RTE was inferior to transient elastography;[28] however, other studies have reported contrasting results.[19] The reason for this variability is probably because RTE technology and the equations used to calculate tissue elasticity are rapidly changing. The utility of elastic ratio, another RTE method for evaluation of liver fibrosis, was reported.[20] The elastic ratio is the ratio between the tissue compressibility of the liver and that of the intrahepatic small vessel. The AUROC of elastic ratio for predicting advanced fibrosis was 0.94 and was superior to LF index. Further, ARFI and real-time shear wave elastography were reported to have a high diagnostic accuracy of liver fibrosis.[10,11,29] There are currently no studies that directly compare LF index and those methods for diagnostic value of liver fibrosis. Therefore, further studies are needed to fully explore the potential of RTE, especially with regard to LF index.

Our study had several limitations. The number of patients with advanced fibrosis was small. The potential of LF index to differentiate patients with F3 and F4 needs to be explored with a large number of patients. Further, validation study is needed to evaluate the diagnostic accuracy of fibrosis stage, especially in comparison with other modalities.

In conclusion, LF index calculated by RTE is useful for predicting liver fibrosis, and diagnostic accuracy of LF index is superior to that of serum fibrosis markers.

Table 4 Diagnostic performance of LF index and serum fibrosis markers

	F0–2 vs F3–4					F0–1 vs F2–4				
	AUROC	Sensitivity (%)	Specificity (%)	PPV (%)	NPV (%)	AUROC	Sensitivity (%)	Specificity (%)	PPV (%)	NPV (%)
LF index	0.84	90.6	71.1	54.7	95.2	0.81	84.3	70.3	69.4	84.9
Platelets	0.82	87.5	66.3	50.0	93.2	0.73	80.4	59.4	61.2	79.2
FIB-4 index	0.80	71.9	81.9	60.5	88.3	0.79	54.9	90.6	82.3	71.6
APRI	0.76	87.5	61.4	46.7	92.7	0.78	64.7	85.9	78.6	75.3

APRI, aspartate aminotransferase/platelet ratio index; AUROC, area under the receiver-operator curve; NPV, negative predictive value; PPV, positive predictive value.

ACKNOWLEDGMENT

THIS STUDY WAS supported by a Grant-in-Aid from Ministry of Health, Labor, and Welfare, Japan.

REFERENCES

1 Serfaty L, Aumaitre H, Chazouilleres O *et al.* Determinants of outcome of compensated hepatitis C virus-related cirrhosis. *Hepatology* 1998; **27**: 1435–40.
2 Benvegnu L, Gios M, Boccato S, Alberti A. Natural history of compensated viral cirrhosis: a prospective study on the incidence and hierarchy of major complications. *Gut* 2004; **53**: 744–9.
3 Dienstag JL. The role of liver biopsy in chronic hepatitis C. *Hepatology* 2002; **36**: S152–60.
4 Gebo KA, Herlong HF, Torbenson MS *et al.* Role of liver biopsy in management of chronic hepatitis C: a systematic review. *Hepatology* 2002; **36**: S161–72.
5 Namiki I, Nishiguchi S, Hino K *et al.* Management of hepatitis C; Report of the Consensus Meeting at the 45th Annual Meeting of the Japan Society of Hepatology (2009). *Hepatol Res* 2010; **40**: 347–68.
6 Bedossa P, Dargere D, Paradis V. Sampling variability of liver fibrosis in chronic hepatitis C. *Hepatology* 2003; **38**: 1449–57.
7 Intraobserver and interobserver variations in liver biopsy interpretation in patients with chronic hepatitis C. The French METAVIR Cooperative Study Group. *Hepatology* 1994; **20**: 15–20.
8 Sandrin L, Fourquet B, Hasquenoph JM *et al.* Transient elastography: a new noninvasive method for assessment of hepatic fibrosis. *Ultrasound Med Biol* 2003; **29**: 1705–13.
9 Friedrich-Rust M, Ong MF, Martens S *et al.* Performance of transient elastography for the staging of liver fibrosis: a meta-analysis. *Gastroenterology* 2008; **134**: 960–74.
10 Friedrich-Rust M, Wunder K, Kriener S *et al.* Liver fibrosis in viral hepatitis: noninvasive assessment with acoustic radiation force impulse imaging versus transient elastography. *Radiology* 2009; **252**: 595–604.
11 Palmeri ML, Wang MH, Rouze NC *et al.* Noninvasive evaluation of hepatic fibrosis using acoustic radiation force-based shear stiffness in patients with nonalcoholic fatty liver disease. *J Hepatol* 2011; **55**: 666–72.
12 Williams AL, Hoofnagle JH. Ratio of serum aspartate to alanine aminotransferase in chronic hepatitis. Relationship to cirrhosis. *Gastroenterology* 1988; **95**: 734–9.
13 Wai CT, Greenson JK, Fontana RJ *et al.* A simple noninvasive index can predict both significant fibrosis and cirrhosis in patients with chronic hepatitis C. *Hepatology* 2003; **38**: 518–26.
14 Lin ZH, Xin YN, Dong QJ *et al.* Performance of the aspartate aminotransferase-to-platelet ratio index for the staging of hepatitis C-related fibrosis: an updated meta-analysis. *Hepatology* 2011; **53**: 726–36.
15 Sterling RK, Lissen E, Clumeck N *et al.* Development of a simple noninvasive index to predict significant fibrosis in patients with HIV/HCV coinfection. *Hepatology* 2006; **43**: 1317–25.
16 Vallet-Pichard A, Mallet V, Nalpas B *et al.* FIB-4: an inexpensive and accurate marker of fibrosis in HCV infection. comparison with liver biopsy and fibrotest. *Hepatology* 2007; **46**: 32–6.
17 Tamaki N, Kurosaki M, Tanaka K *et al.* Noninvasive estimation of fibrosis progression overtime using the FIB-4 index in chronic hepatitis C. *J Viral Hepat* 2013; **20**: 72–6.
18 Friedrich-Rust M, Ong MF, Herrmann E *et al.* Real-time elastography for noninvasive assessment of liver fibrosis in chronic viral hepatitis. *AJR Am J Roentgenol* 2007; **188**: 758–64.
19 Morikawa H, Fukuda K, Kobayashi S *et al.* Real-time tissue elastography as a tool for the noninvasive assessment of liver stiffness in patients with chronic hepatitis C. *J Gastroenterol* 2011; **46**: 350–8.
20 Koizumi Y, Hirooka M, Kisaka Y *et al.* Liver fibrosis in patients with chronic hepatitis C: noninvasive diagnosis by means of real-time tissue elastography – establishment of the method for measurement. *Radiology* 2011; **258**: 610–17.

21 Tatsumi C, Kudo M, Ueshima K *et al.* Non-invasive evaluation of hepatic fibrosis for type C chronic hepatitis. *Intervirology* 2010; 53: 76–81.
22 Tomeno W, Yoneda M, Imajo K *et al.* Evaluation of the Liver Fibrosis Index calculated by using real-time tissue elastography for the non-invasive assessment of liver fibrosis in chronic liver diseases. *Hepatol Res* 2012; 12: 12023.
23 Bedossa P, Poynard T. An algorithm for the grading of activity in chronic hepatitis C. The METAVIR Cooperative Study Group. *Hepatology* 1996; 24: 289–93.
24 Castera L, Foucher J, Bernard PH *et al.* Pitfalls of liver stiffness measurement: a 5-year prospective study of 13,369 examinations. *Hepatology* 2010; 51: 828–35.
25 Fraquelli M, Rigamonti C, Casazza G *et al.* Reproducibility of transient elastography in the evaluation of liver fibrosis in patients with chronic liver disease. *Gut* 2007; 56: 968–73.
26 Arena U, Vizzutti F, Abraldes JG *et al.* Reliability of transient elastography for the diagnosis of advanced fibrosis in chronic hepatitis C. *Gut* 2008; 57: 1288–93.
27 Rizzo L, Calvaruso V, Cacopardo B *et al.* Comparison of transient elastography and acoustic radiation force impulse for non-invasive staging of liver fibrosis in patients with chronic hepatitis C. *Am J Gastroenterol* 2011; 106: 2112–20.
28 Colombo S, Buonocore M, Del Poggio A *et al.* Head-to-head comparison of transient elastography (TE), real-time tissue elastography (RTE), and acoustic radiation force impulse (ARFI) imaging in the diagnosis of liver fibrosis. *J Gastroenterol* 2012; 47: 461–9.
29 Ferraioli G, Tinelli C, Dal Bello B, Zicchetti M, Filice G, Filice C. Accuracy of real-time shear wave elastography for assessing liver fibrosis in chronic hepatitis C: a pilot study. *Hepatology* 2012; 56: 2125–33.

Gastroenterology 2014;146:222–232

BASIC AND TRANSLATIONAL—LIVER

Leptin Receptor Somatic Mutations Are Frequent in HCV-Infected Cirrhotic Liver and Associated With Hepatocellular Carcinoma

Atsuyuki Ikeda,[1] Takahiro Shimizu,[1] Yuko Matsumoto,[1] Yosuke Fujii,[1] Yuji Eso,[1] Tadashi Inuzuka,[1] Aya Mizuguchi,[1] Kazuharu Shimizu,[2] Etsuro Hatano,[3] Shinji Uemoto,[3] Tsutomu Chiba,[1] and Hiroyuki Marusawa[1]

Departments of [1]Gastroenterology and Hepatology and [3]Surgery, Graduate School of Medicine, and [2]Department of Nanobio Drug Discovery, Graduate School of Pharmaceutical Sciences, Kyoto University, Kyoto, Japan

See Covering the Cover synopsis on page 2.

BACKGROUND & AIMS: Hepatocellular carcinoma develops in patients with chronic hepatitis or cirrhosis via a stepwise accumulation of various genetic alterations. To explore the genetic basis of development of hepatocellular carcinoma in hepatitis C virus (HCV)-associated chronic liver disease, we evaluated genetic variants that accumulate in nontumor cirrhotic liver. **METHODS:** We determined the whole exome sequences of 7 tumors and background cirrhotic liver tissues from 4 patients with HCV infection. We then performed additional sequencing of selected exomes of mutated genes, identified by whole exome sequencing, and of representative tumor-related genes on samples from 22 cirrhotic livers with HCV infection. We performed in vitro and in vivo functional studies for one of the mutated genes. **RESULTS:** Whole exome sequencing showed that somatic mutations accumulated in various genes in HCV-infected cirrhotic liver tissues. Among the identified genes, the leptin receptor gene (*LEPR*) was one of the most frequently mutated in tumor and nontumor cirrhotic liver tissue. Selected exome sequencing analyses detected *LEPR* mutations in 12 of 22 (54.5%) nontumorous cirrhotic livers. In vitro, 4 of 7 (57.1%) *LEPR* mutations found in cirrhotic livers reduced phosphorylation of STAT3 to inactivate LEPR-mediated signaling. Moreover, 40% of Lepr-deficient (C57BL/KsJ-*db/db*) mice developed liver tumors after administration of thioacetamide compared with none of the control mice. **CONCLUSIONS:** Based on analysis of liver tissue samples from patients, somatic mutations accumulate in *LEPR* in cirrhotic liver with chronic HCV infection. These mutations could disrupt LEPR signaling and increase susceptibility to hepatocarcinogenesis.

Keywords: Liver Cancer; Whole Exome Sequencing; Genetics; STAT3.

Chronic inflammation plays an important role in the development of various human cancers. Indeed, many human cancers are closely associated with chronic inflammation, such as *Helicobacter pylori*–associated gastric cancer and inflammatory bowel disease–associated colorectal cancer.[1,2] On the other hand, tumor cells are believed to be generated by a stepwise accumulation of genetic alterations in various tumor-related genes during the process of inflammation-associated carcinogenesis.[3–6] Thus, it is reasonable to assume that somatic mutations latently accumulate in inflamed tissues, where the risk of tumorigenesis is high. Consistent with this hypothesis, several studies have shown frequent somatic mutations in nontumorous inflammatory tissues.[7,8] To clarify the mechanisms of inflammation-associated carcinogenesis, it is important to unveil the genetic alterations that occur in the inflamed tissues before tumor development. The diversity of mutated genes and the low frequency of genetic alterations compared with tumor tissues, however, are obstacles to revealing the landscape of accumulated genetic aberrations in chronically inflamed nontumorous tissues.

Several possible molecular mechanisms have been proposed for the genetic alterations occurring in the inflammatory condition.[9] We recently showed that the expression of activation-induced cytidine deaminase (AID), a DNA/RNA mutator enzyme family member, links inflammation to an enhanced susceptibility to genetic aberration during the development of various gastrointestinal and hepatobiliary cancers.[10–12] One clear example of inflammation-associated cancer is human hepatocellular carcinoma (HCC). HCC arises in the background of chronic inflammation caused by hepatitis C virus (HCV) infection.[13] We showed that aberrant AID expression triggered by HCV infection and the resultant inflammatory response leads to the generation of somatic mutations in various tumor-related genes in the inflamed liver tissues.[14,15] The target genes of AID-mediated mutagenesis in the inflamed hepatocytes, however, remain unclear.

Recent advances in sequencing technology have enabled us to reveal the whole picture of human genome sequences in association with the risk of development of a variety of human diseases, including cancers.[16,17] Whole exome capture

Abbreviations used in this paper: **AID, activation-induced cytidine deaminase; HCC, hepatocellular carcinoma; HCV, hepatitis C virus; Ig, immunoglobulin; TAA, thioacetamide.**

0016-5085/$36.00
http://dx.doi.org/10.1053/j.gastro.2013.09.025

has identified several candidate driver genes in various human cancers.[18–20] Although deep sequencing on tumor tissues provides the most comprehensive analysis of the cancer genome, the genetic alterations accumulated in chronically inflamed tissues might provide an additional opportunity to clarify the early genetic changes required for carcinogenesis. In the present study, we applied whole exome sequencing to not only the tumor but also nontumorous liver tissues infected with HCV and found that somatic mutations of the leptin receptor gene (*LEPR*) latently underlie a subset of the cirrhotic liver tissues, providing the putative genetic basis for HCV-associated hepatocarcinogenesis.

Materials and Methods

Whole Exome Capture and Massively Parallel Sequencing

Massively parallel sequencing was performed as described previously.[21,22] Fragmented DNA (more than 5 μg) was used to prepare each DNA sequencing library. The DNA libraries were prepared according to the instructions provided with the Illumina Preparation Kit (Illumina, San Diego, CA). Whole exome sequence capture was then performed using SeqCap EZ Human Exome Library v2.0 (Roche, Madison, WI) according to the manufacturer's instructions. Cluster generation was performed on the Illumina cluster station (using their TruSeq PE Cluster Kit v5). Paired-end sequence for 2 $\times$ 76 base pairs was performed on the Illumina Genome Analyzer IIx (using their SBS Kits v5). Data collection and base calling were performed using SCS v2.9/RTA 1.9, and the resultant data files were converted to the FASTQ format.

Selected Exome Capture and Massively Parallel Sequencing

Fragmented DNA (1 μg) was used to prepare each DNA sequencing library. The DNA libraries were prepared using TruSeq DNA Sample Prep Kits (Illumina) according to the manufacturer's protocol. Selected gene capture (*TP53*, *CTNNB1*, *LEPR*) was performed using the SeqCap EZ Choice library (Roche) according to the manufacturer's recommendations. Cluster generation and multiplexed paired-end sequencing for 2 $\times$ 71 + 7 base pairs was performed as described previously. Data collection and base calling were performed as described previously and demultiplexed using CASAVA version 1.8.2 software (Illumina) with the default settings.

Sequence data analysis and variant filtering, patients, cell culture and transfection, immunoblotting analysis, and animal experiments are described in Supplementary Methods and Supplementary Figures 1 and 2.

Results

Whole Exome Sequencing Identified the Mutation Signature of Synchronous HCCs in Patients With Chronic HCV Infection

To explore the genetic basis of HCV-associated hepatocarcinogenesis, we first determined the whole exome sequences in matched pairs of HCC and background liver tissues obtained from 4 patients with chronic HCV infection (Supplementary Table 1, patients 1–4). Three of these patients had multiple HCCs, and one had a solitary HCC in the liver. To compare the mutation signature in synchronous HCCs that developed in the same background liver, we determined the whole exome sequences of 2 representative HCCs in 3 cases and a solitary HCC in the remaining case (Figure 1). These 7 HCCs from 4 patients comprised 2 well-differentiated and 5 moderately differentiated HCCs, and the background liver tissue showed the histological characteristics of cirrhosis. To subtract the normal variants of each individual from the somatic mutations, we also determined the whole exome sequences of matched peripheral lymphocytes in each patient.

On average, we generated approximately 3.1 gigabases of sequence per sample, 80.1% of which were aligned with the human reference genome (Human Genome Build 37.3), and the mean coverage in the targeted regions was 33.8-fold (Supplementary Table 2). The variant filtering process is summarized in Supplementary Figure 1, and the overall error rate in our current platform was confirmed to be less than 0.2%, as described previously.[21] Overall, a total of 970 nucleotide positions in 768 different genes were mutated at a frequency of more than 20% of reads in the 7 HCC tissues (Supplementary Table 3). Among them, 79 genes were recurrently mutated in 2 or more tumor tissues (data not shown). These genes included representative tumor-related genes associated with HCC such as *TP53* (mutated in 2 of 7 tumors). Pathway analyses using Kyoto Encyclopedia of Genes and Genomes (KEGG; http://www.genome.jp/kegg/) revealed that metabolic pathway–related genes were most frequently damaged in HCC tissues (5 of 7 tumors) (Supplementary Table 4).

Interestingly, the mutation signature was remarkably different between the synchronously developed HCCs in each patient (Figure 1). In patient 3, none of the genes were commonly mutated in the 2 tumors examined, while 29 and 225 genes acquired independent somatic mutations in each tumor, respectively. In contrast, 32 genes (64.0% of mutated genes of HCC 1 in patient 1) and 9 (24.3% of mutated genes of HCC 1 in patient 2) were commonly mutated in the synchronously developed HCCs of those patients, indicating that the synchronous HCCs that developed in patient 1 or 2 shared a common pattern of genetic aberrations. These findings may suggest that the synchronous tumors in patients 1 and 2 were derived from common tumor-precursor cells or developed through intrahepatic metastasis, whereas the tumors in patient 3 developed independently in a multicentric manner.

Somatic Mutations Accumulated in the Cirrhotic Liver With HCV Infection

Whole exome sequencing also revealed a large number of nucleotide alterations in nontumorous cirrhotic liver tissues. In some cases, the total number of mutated genes in nontumorous liver was higher than that in tumor tissues, while the mutation frequency in nontumorous tissues tended to be lower than that in the matched tumor tissues (Figure 2). Sorting Intolerant From Tolerant (SIFT) functional impact predictions (http://provean.jcvi.org/index.php) revealed that the mean percentage of somatic

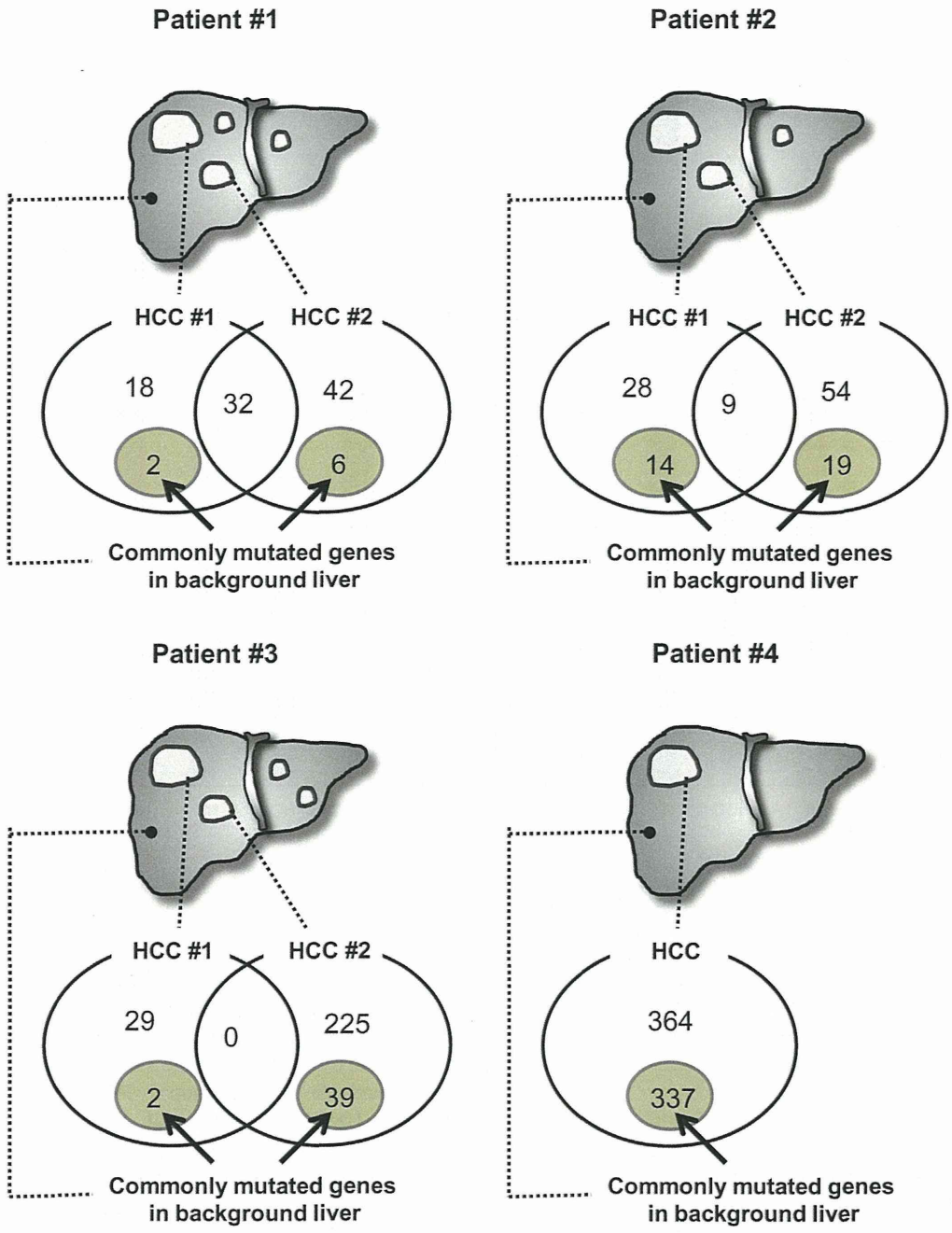

Figure 1. Schematic diagram showing the number of mutated genes in tumors and the number of genes commonly mutated in both tumor and the matched nontumorous liver tissues. Patients 1, 2, and 3 had synchronously developed HCCs, and patient 4 had a solitary HCC. Venn diagrams represent the number of mutated genes in each HCC tissue determined by whole exome sequencing. The numbers of genes commonly mutated in the synchronously developed multiple HCCs were 32, 9, and 0 in patients 1, 2, and 3, respectively. Among the mutated genes in HCC (at a frequency of more than 20% of reads), the number of genes commonly mutated in both HCC and matched nontumorous background liver (at a frequency of more than 5% of reads) is shown in *shaded circles*.

mutations predicted to be "damaging" in tumorous and nontumorous tissues was 20.4% and 13.1%, respectively, suggesting that somatic mutations that accumulated in nontumorous tissues included "passenger" mutations with less functional significance more frequently than those that accumulated in tumor tissues (Supplementary Table 3). We also identified a total of 448 indels in 7 HCC tissues (Supplementary Table 5), while fewer indels were detected in all of the nontumorous cirrhotic liver tissues examined (Supplementary Table 6). Consistent with previous studies,[19] we found that one-third of the mutations that accumulated in the exome sequences of HCC tissues were enriched as C>T; G>A transition, followed by A>G; T>C. Similar to tumor tissues, C>T; G>A transition mutations were most frequently detected in nontumorous cirrhotic tissues (Supplementary Figure 3).

The aim of this study was to identify the somatic mutations in the nontumorous HCV-positive cirrhotic liver that may contribute to tumorigenesis. Therefore, we focused on the genes commonly mutated in both tumor and nontumorous liver tissues from the same patient. Because few genes commonly acquired somatic mutations with a frequency of more than 20% both in the tumor and the matched nontumorous liver tissues, we selected potential somatic mutations in nontumorous tissues that represented more than 5% of the total reads for further evaluation

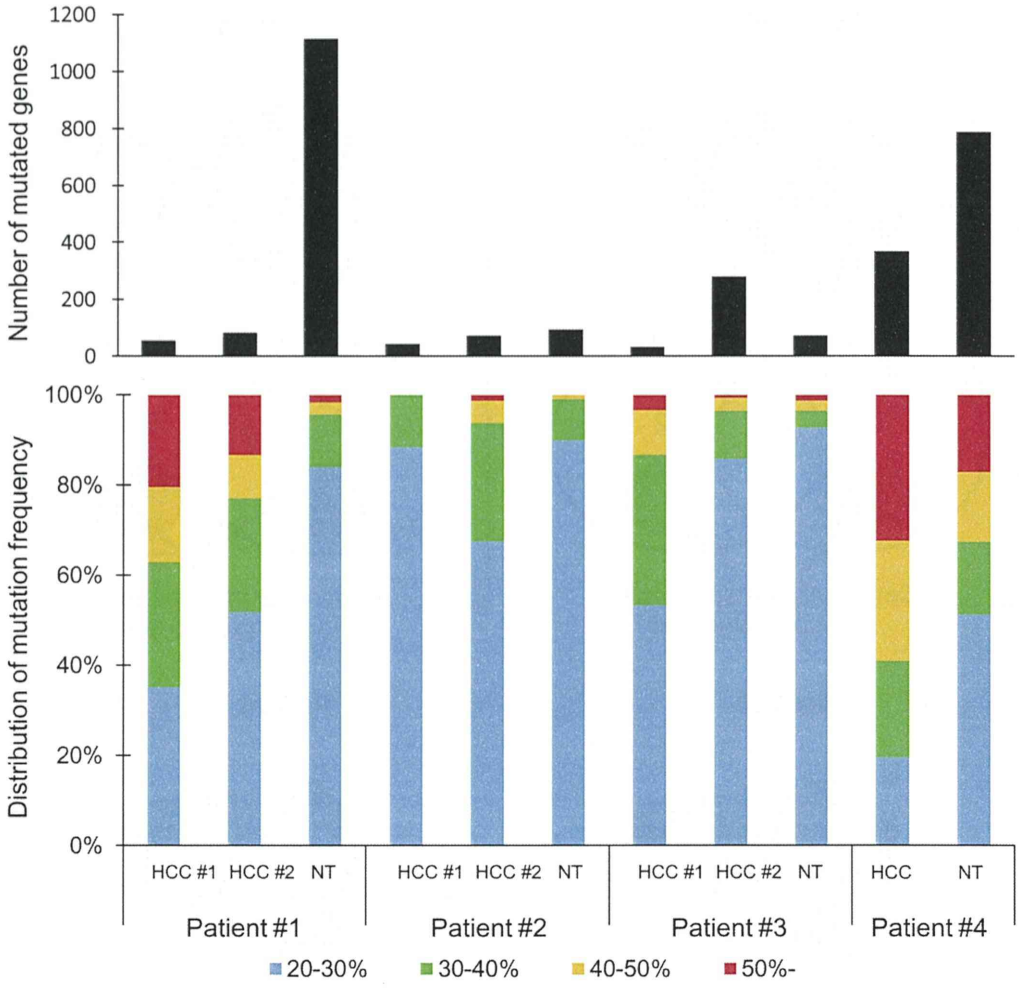

Figure 2. The number of mutated genes and the distribution of mutation frequency in tumor and nontumorous cirrhotic liver tissues. The number of mutated genes (*upper panel*) and the distribution of mutation frequency (*lower panel*) detected by whole exome sequencing in each sample are shown (at a frequency of more than 20% of reads). Patients 1, 2, and 4 had more mutated genes in nontumorous liver tissue than those in HCC, while the mutation frequency at each nucleotide position in the majority of nontumorous cirrhotic liver tissues was <30%. NT, nontumorous cirrhotic liver.

(Supplementary Figure 1). The 5% threshold in nontumorous liver was chosen because common polymorphisms in each patient were excluded by determining the nucleotide changes with a frequency of more than 5% in the matched normal samples, such as peripheral lymphocytes.[18,23]

Based on these criteria, nucleotide positions that were commonly mutated in both the tumor (at a frequency of more than 20% of reads) and the matched background liver (at a frequency of more than 5% of reads)of each patient were detected (Figure 1). Among them, we focused on 40 mutations that result in amino acid changes (Supplementary Table 7) and found that only 2 genes, *LEPR* and *ZNF408*, were recurrently mutated with a frequency greater than 5% of reads in nontumorous cirrhotic livers from 2 of the 4 patients (listed as the top 2 genes in Supplementary Table 7). Of these 2 genes, we focused on *LEPR*, which has mutations that have been correlated with various human diseases, such as obesity and metabolic disorders.[24]

Identification of LEPR as the Recurrently Mutated Gene in Cirrhotic Livers With HCV Infection

We designed a selected sequence capture system that enabled us to enrich the whole exonic sequences of the *LEPR* followed by deep sequencing. In addition, selected exonic capture of *TP53* and *CTNNB1*, the representative driver genes for hepatocarcinogenesis,[19,20,25] was performed on the same cohort. Accordingly, the selected exonic sequencing was applied to 22 additional HCV-positive cirrhotic liver tissues, 10 HCC tissues, and matched peripheral lymphocytes from 22 patients (Supplementary Table 1, patients 5–26). Selected exome sequencing generated a mean coverage of 996-, 1656-, and 2348-fold on *LEPR*, *TP53*, and *CTNNB1*, respectively (Supplementary Table 8). The variant filtering process is summarized in Supplementary Figure 2, and we detected both high-frequency (at a frequency of more than 20% of reads) and low-frequency (at a frequency of 1%–20% of reads) mutations separately.

High-frequency mutations in *TP53* and *CTNNB1* were detectable in 1 of 10 (10%) and 1 of 10 (10%) of the HCCs, respectively (Table 1), and these rates in the HCCs were consistent with recent deep-sequencing studies.[19,20] None of the nontumorous liver tissues possessed high-frequency mutations in *TP53* or *CTNNB1*; however, low-frequency mutations of *TP53* and *CTNNB1* were detected in 17 of 22 (77.3%) and 12 of 22 (54.5%) of the nontumorous livers, respectively. These findings indicated that somatic mutations in the representative cancer driver genes latently

Table 1. Number of Tumor Tissues and Nontumorous Cirrhotic Liver Tissues With Somatic Mutations at High and Low Frequencies in *TP53*, *CTNNB1*, and *LEPR*

	LEPR	*TP53*	*CTNNB1*
High-frequency mutations (>20%)			
Tumor (n = 10)	0	1	1
Nontumor (n = 22)	1[a]	0	0
Low-frequency mutations (1%–20%)			
Tumor (n = 10)	9	8	9
Nontumor (n = 22)	12[a]	17	12

[a]One patient had both high-frequency and low-frequency mutations in *LEPR*.

accumulated with a relatively low frequency in the cirrhotic livers with HCV infection.

Interestingly, we also found high- and/or low-frequency mutations in *LEPR* in both tumor and nontumorous liver tissues. Indeed, 9 of 10 (90%) tumors and 12 of 22 (54.5%) nontumorous cirrhotic livers possessed high- and/or low-frequency mutations in *LEPR* (Table 1). Notably, some somatic mutations were commonly detected in different positions of the same patient's liver. For example, C1084T (reference position: 65557165) mutations of *LEPR* were detected in the right, left, and caudate lobes of one patient (Supplementary Table 1, patient 11), suggesting that some of the hot spots of the acquired somatic mutations in the *LEPR* gene are commonly present in hepatocytes of the same liver underlying HCV infection. On the other hand, no mutations in *LEPR* were identified by deep sequencing analysis of noncirrhotic liver tissues from patients with chronic HCV infection or liver tissue from patients without HCV infection. (Supplementary Table 9). To confirm the somatic mutations present in *LEPR* in the nontumorous liver, we validated the candidate mutations by Sanger sequencing. For this purpose, we determined the sequences of exons 9 and 10 of *LEPR* of at least 50 randomly picked clones that were amplified from the nontumorous liver tissues of each patient. Although it was difficult to detect all the low-frequency mutations using the conventional cloning-sequencing method, we confirmed that somatic mutations were recurrently accumulated in *LEPR* of nontumorous cirrhotic liver tissues (Supplementary Figure 4).

LEPR Mutations Found in HCV-Positive Cirrhotic Liver Resulted in the Disruption of Downstream Signaling

Selected exome sequencing detected low-frequency mutations at a total of 650 nucleotide positions of *LEPR* in 12 of 22 (54.5%) HCV-positive cirrhotic liver tissues. Although the nucleotide changes were unevenly distributed throughout the whole *LEPR* exonic sequences, we detected 67 nucleotide alterations at the immunoglobulin (Ig) domain of *LEPR*, 38 of which (56.7%) were recurrently mutated in 2 or more patients (Figure 3*A*). Among them, nonsynonymous mutations that caused the amino acid changes were detected at 62 of the 67 (92.5%) nucleotide positions, and 10 of the 62 were also mutated in at least one HCC tissue examined in this study. Histological examination revealed no significant association between the presence of *LEPR* mutations and the level of fatty changes in the liver tissue (data not shown).

To explore the functional relevance of *LEPR* mutations detected in HCV-positive cirrhotic liver tissues, we randomly selected 7 *LEPR*s with a mutated Ig domain from 62 nonsynonymously mutated *LEPR*s and examined the downstream signaling properties of the mutated *LEPR* in vitro.

Accordingly, we subcloned the mutated *LEPR*s and constructed expression plasmids encoding those mutant *LEPR*s (Figure 3*B*). We first confirmed that only a small amount of endogenous LEPR expression was observed in both HEK293 and HepG2 cells (Supplementary Figure 5) and the induction of the phosphorylation of STAT3 by wild-type *LEPR* in the presence of recombinant human leptin (Figure 3*C*). In contrast, 4 of 7 (57.1%) mutations in the Ig domain of *LEPR* resulted in the reduction or loss of STAT3 phosphorylation in vitro (Figure 3*C*). To clarify the functional significance of *LEPR* mutations, the cell proliferation rate was determined in HepG2 cells expressing either wild-type or mutated *LEPR*s that were identified in HCV-positive cirrhotic liver tissues using the lentivirus system.[26] Up-regulation of cyclin D1 and/or E transcripts as well as enhanced cell proliferation were observed in the cells with expression of the mutated *LEPR* gene compared with wild-type cells, while there was no difference in the expression levels and subcellular localization between wild-type and mutated LEPR protein (Supplementary Figure 6). These findings indicate that some of the somatic mutations that latently accumulated in the Ig domain of *LEPR* of the cirrhotic liver tissue might cause dysfunction of LEPR-mediated signaling in the cells with those somatic mutations.

LEPR Dysfunction Enhanced Susceptibility to Tumorigenesis

To determine the functional relevance of LEPR dysfunction on development of liver cancer, we examined whether disruption of the LEPR gene contributes to liver tumorigenesis using a genetically altered mouse model, the Lepr-deficient C57BL/KsJ-*db/db* mouse (hereafter referred to as *db/db* mouse).[27] Thioacetamide (TAA), a putative carcinogen, is well established to induce liver fibrosis and tumorigenesis in a murine model.[28] Thus, we conducted an assay to evaluate whether LEPR insufficiency alters the effects of TAA-mediated tumorigenesis. Accordingly, TAA was prepared at a concentration of 0.02%, a relatively low dose compared with the carcinogenic dose,[29] and administered in drinking water to mice for 24 weeks. The body weight of the *db/db* mice was about twice that of their lean littermates, and *db/db* mice had hepatomegaly even after normalizing the liver weight to the body weight (Figure 4*A*). Histological

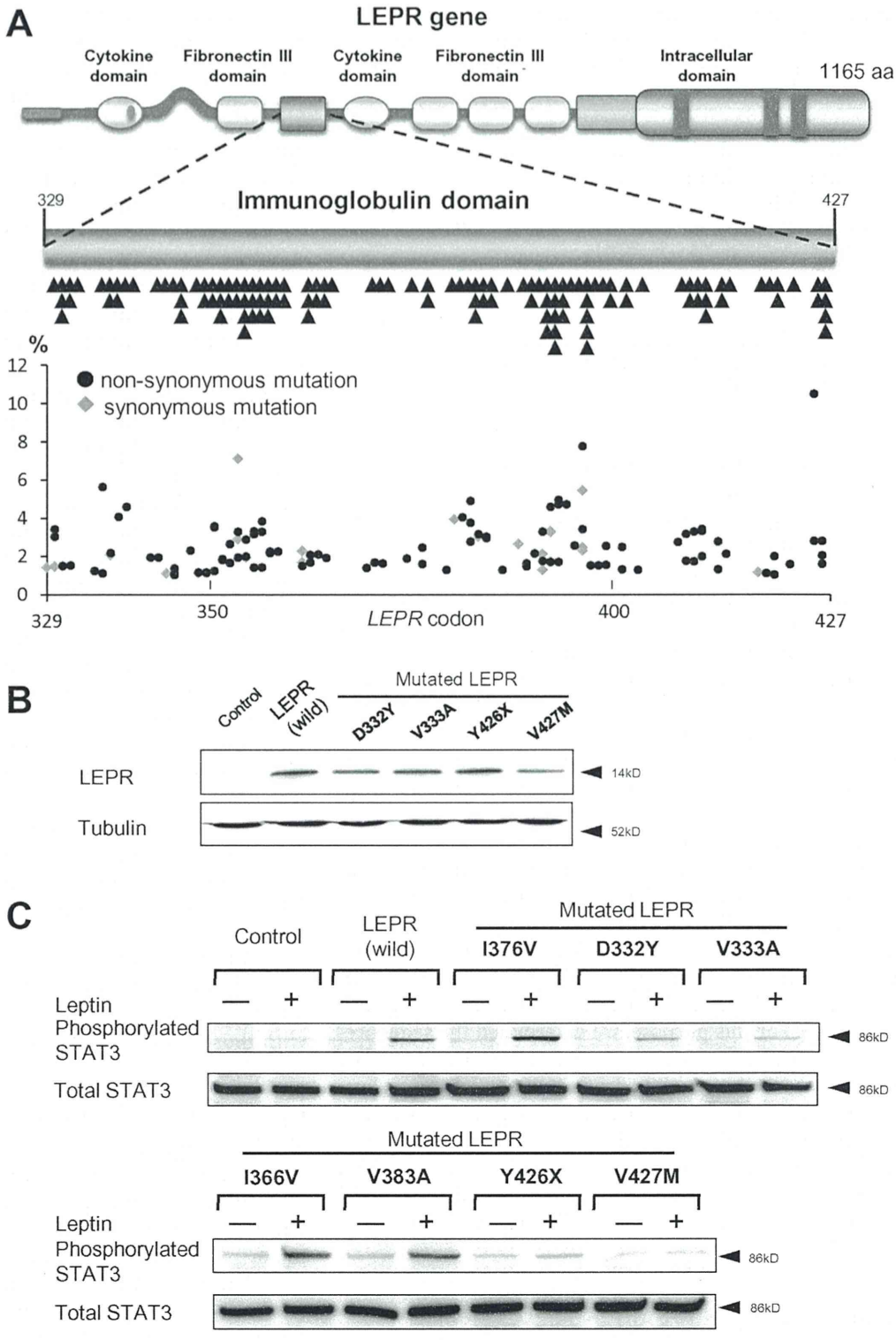

Figure 3. Distribution of mutations in the *LEPR* sequence in HCV-positive cirrhotic liver tissues. (*A*) Schematic diagram of the LEPR gene (*top panel*) and the Ig domain (*middle panel*). Mutated positions in the Ig domain are indicated by *black triangles*. A total of 38 of 67 (56.7%) mutated nucleotide positions of the Ig domain were recurrently mutated in 2 or more HCV-positive cirrhotic liver tissues. Frequencies of non-synonymous (*black circles*) and synonymous (*gray diamonds*) mutations at each nucleotide position of the Ig domain of each sample are shown (*lower panel*). Nonsynonymous mutations were detected at 62 of the 67 nucleotide positions. (*B* and *C*) HEK293 cells were transfected with constructs encoding wild-type or representative various mutated *LEPR*s that were identified in HCV-positive cirrhotic liver tissues. Control: empty vector. (*B*) Immunoblotting was performed on the lysate of the cells expressing either wild-type or a mutated Ig domain (D332Y, V333A, Y426X, and V427M) of the *LEPR* gene using anti-Myc antibodies. (*C*) After transfection, the cells were treated with or without recombinant leptin protein. Total protein was isolated and immunoblot analysis was performed using anti–phospho-STAT3 (*upper panel*) and anti–total STAT3 (*lower panel*).

examination revealed the accumulation of lipids within individual hepatocytes in the *db/db* mouse liver, a typical feature of steatosis (Figure 4*A*).

After administering TAA, blood levels of alanine aminotransferase were substantially elevated in *db/db* mice compared with control mice (Supplementary Table 10). Consistently, histological examination revealed that inflammatory activity was more severe in the liver of *db/db* mice than in the liver of control mice (Figure 4*B*). None of the control mice treated with TAA showed tumorigenesis 24 weeks after administration of TAA. In contrast, macroscopic liver nodules developed in 4 of 10 (40%) *db/db* mice